ACS NANOSCIENCE Au
AN OPEN ACCESS JOURNAL OF THE AMERICAN CHEMICAL SOCIETY

pubs.acs.org/nanoau
Article

Intermolecular Interactions and Quantum Interference Effects in Molecular Junctions

Louise O. H. Hyllested, Idunn Prestholm, and Gemma C. Solomon*

Cite This: ACS Nanosci. Au 2024, 4, 426–434
Read Online

ABSTRACT: Destructive quantum interference (DQI) leads to a decrease in the conductance of certain well-documented molecules. Experimental observations have revealed both direct and indirect manifestations of DQI, although a comprehensive understanding of the underlying causes of these distinct outcomes remains elusive. In both cases, DQI lowers the conductance, but only the direct case exhibits a characteristic V-shaped dip in differential conductance. Currently, the direct signature has exclusively been observed in monolayers and gated single-molecule systems. In this study, we employ density functional theory to elucidate a plausible explanation for the absence of a direct DQI signature in single molecules. Specifically, we attribute the direct DQI signature to a resonance shift induced by intermolecular interactions, which are absent in the individual molecules. By illustrating the impact of these intermolecular interactions, we emphasize the need for explicit treatment of intermolecular interactions when simulating monolayers.

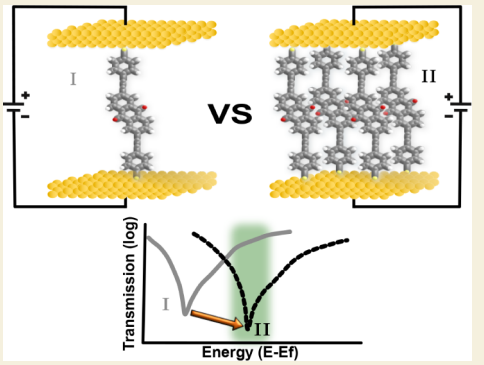

KEYWORDS: *quantum interference, self-assembled monolayer, conductance, density functional theory, charge transport.*

INTRODUCTION

Over the last 15 years, destructive quantum interference (DQI) effects have become accepted as an uncontroversial characteristic of electron transport through some classes of organic molecules, such as anthraquinone and oligo-(phenyleneethynylene) derivatives.[1−3]

When present, DQI hinders the flow of electrons across the molecule, resulting in the molecule exhibiting insulating properties. Similar to the phenomenon of destructive interference in water, DQI can be understood as a cancellation of waves. Despite its widespread presence in the literature, we still do not completely understand how this effect manifests in different molecular environments.

In general, DQI in molecules is observed as a suppressed conductance. In the most extreme case, complete suppression of the conductance could occur; however, in practice DQI results in incomplete suppression of the conductance and some low-level conductance is observed. In one of the earliest experimental reports of DQI in molecules, Guédon et al.,[4] described a "direct" signature of DQI as a V-shaped dip in the differential conductance (dI/dV). As also noted in that work, the absence of a V-shaped dip in dI/dV is not, however, an indication that DQI is absent but rather that it only manifests in a less definitive way as suppressed conductance. To distinguish between different observations of DQI, here we employ the terms "direct" and "indirect". The direct observation of DQI is characterized by the V-shaped dip in the dI/dV, while the indirect observation merely presents as suppressed conductance independent of line shape. This contrast is illustrated in Figure 1e,f.

Similar to experimental observations, the DQI can also be seen in calculated electronic transmission. In this context, DQI manifests as a dip in the transmission spectrum, which can be sharp or broad and may or may not be energetically aligned with the electrode Fermi energy. The direct signature in dI/dV will most clearly manifest in the case that DQI is leading to a sharp dip near the Fermi energy (Figure 1a). As the sharpness of the dip or the proximity to the Fermi energy decreases, the line shape of dI/dV will change and the system will eventually only exhibit an indirect signature (Figure 1d).

One way to study DQI in molecules is through molecular conductance experiments. These experiments typically focus on either monolayers or single molecules, where the primary distinction lies in the number of molecules involved and, consequently, the resulting molecular environment. When multiple molecules are present, the intermolecular interactions come into play alongside the inherent DQI exhibited by individual molecules.

Several single-molecule experiments have demonstrated the indirect signature of DQI as a general decrease in conductance

Received: July 19, 2024
Revised: September 23, 2024
Accepted: September 24, 2024
Published: October 4, 2024

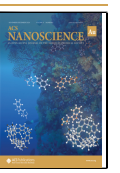

https://doi.org/10.1021/acsnanoscienceau.4c00041
ACS Nanosci. Au 2024, 4, 426–434

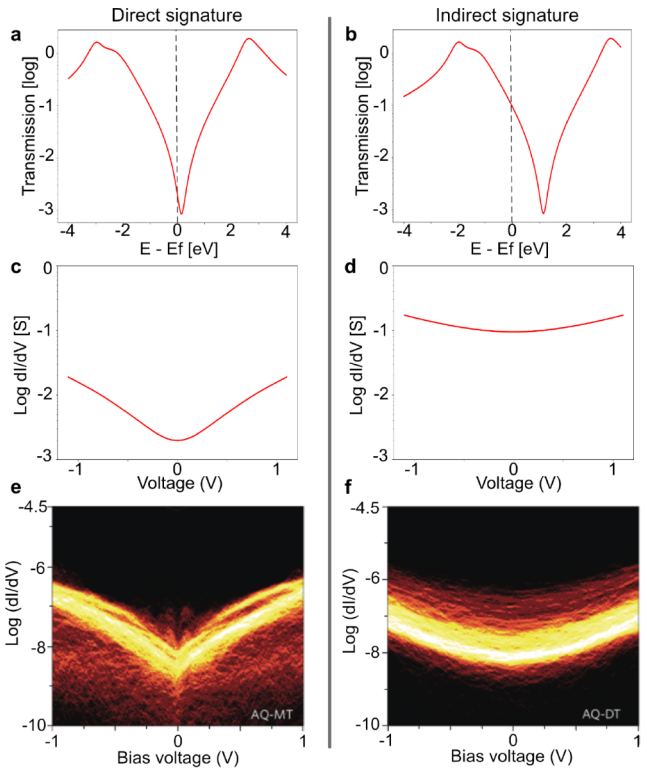

Figure 1. Illustration of transmission for the direct (a) and indirect (b) signatures of DQI. The shift is caused by a change in the onsite energies, from 0 eV in (a) to 1 eV in (b). (c,d) Corresponding dI/dV graphs for the direct (c) and indirect (d) signatures of DQI, respectively. a−d, was calculated using a Hückel model, see Section S1 for further details. (e,f) Experimental conductance measurements of AQ-MT (e) showing a V-shaped dip in the conductance associated with DQI. AQ-DT (f) exhibits a curve associated with either an indirect or no signature of DQI. Both graphs represent logarithmically binned histograms of dI/dV (in Ω^{-1}) versus bias voltage. (e,f) are reproduced with permission from Guédon et al.[4] Copyright 2023 Springer Nature.

without any distinct features.[5−8] In addition, Garner et al.[9] observed the indirect signature of DQI in single molecules, characterized by low conductance and high thermopower. However, direct signatures of DQI in single molecules have only been observed in experiments involving gated junctions.[10,11] The application of gating alters the molecular environment, causing a shift of the DQI into the measurable range. To the best of our knowledge, direct signatures of quantum interference without gating have solely been observed in ensemble junctions.[2,4,12−16] It is worth noting that although an overall low conductance can result from various factors, such as weak connections to the electrodes, a direct signature holds particular importance in confirming the presence of the DQI.

To gain a deeper understanding of the origin of DQI in experiments, theoretical calculations serve as a valuable tool. Theoretically, DQI can be observed in calculations, similar to experiments, as a V-shaped dip in the transmission spectrum, as illustrated in Figure 1a. In 2014, Lykkebo et al.[17] utilized the Hückel model to demonstrate that the interference feature in the transmission spectrum of a single molecule can be shifted by altering the onsite energy of the molecule. In these types of calculations, the transmission around the Fermi energy is the most important, as this region corresponds to what can be probed in experiments. To emphasize the significance of the position of the dip in the transmission spectrum, Figure 1 presents a theoretical depiction of the transmission spectrum and the differential conductance (dI/dV) with varying onsite energies.

As shown by Lykkebo et al., a shift in the onsite energy leads to a corresponding shift of the V-shaped dip in the transmission. This is illustrated by a Hückel model calculation example in Figure 1a,b (see Section S1 for further details). In Figure 1a, the dip aligns with the Fermi energy (0 eV), while, in Figure 1b, it occurs at a higher energy. Examining Figure 1c,d, the plots of dI/dV reveal that only a dip close to the Fermi energy (Figure 1a) results in a V-shaped dip in dI/dV (Figure 1c). By manipulating the onsite energy of the molecule in Hückel calculations, it is possible to shift the interference feature into the measurable range. This example illustrates the distinction between indirect and direct signatures of DQI. Indirect signatures exhibit a dip far from the Fermi energy, while direct signatures feature a dip in the transmission spectrum located at or near the Fermi energy, leading to a dip in the dI/dV. Given our understanding of how DQI can be observed, the question arises as to why the direct signature of DQI has only been detected in monolayers in ungated experiments.

In this study, we focus our investigation on a set of molecules with cross-conjugated and linearly conjugated structures, namely, anthracene-dithiol (AC-DT), anthraquinone-dithiol (AQ-DT), and anthraquinone-monothiol (AQ-MT), depicted in Figure 2. Previous experimental studies[4] have revealed both indirect and direct signatures of DQI in AQ-DT and AQ-MT, respectively. Given that these molecules possess DQI as single entities due to their cross-conjugated nature,[18] they serve as excellent candidates for exploring the influence of intermolecular interactions on DQI.

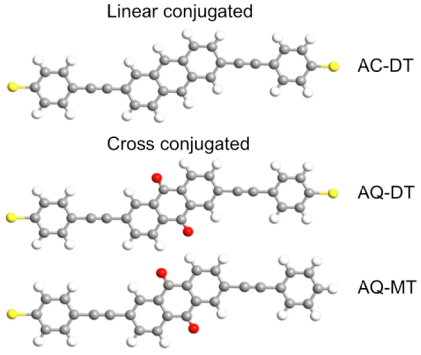

Figure 2. Chemical structures of the molecules included in the study; two cross-conjugated molecules: dithiolated anthraquinone and monothiolated anthraquinone (AQ-DT, AQ-MT) and one linearly conjugated molecule: dithiolated anthracene (AC-DT).

MODEL SYSTEM

To begin our study, we utilized a simple model based on Hückel theory. Since direct signature of DQI has only been observed for monolayers[4,12−16] and gated single-molecule experiments,[10,11] it is likely that molecular interactions play a role in determining whether there is a direct or indirect signature of DQI. To investigate this further, we employ a Hückel model that incorporates two ethene molecules, either

https://doi.org/10.1021/acsnanoscienceau.4c00041
ACS Nanosci. Au 2024, 4, 426−434

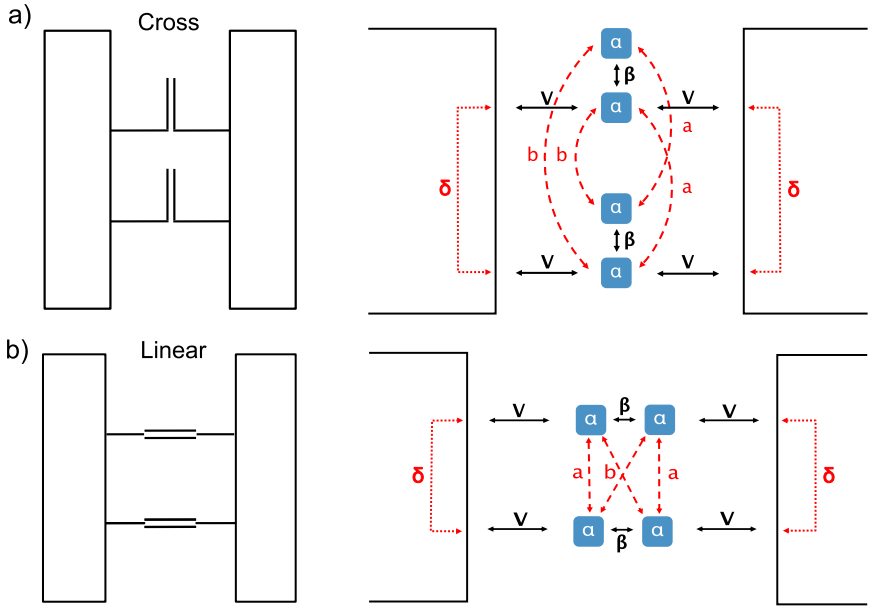

Figure 3. A schematic of the two-molecule linear and cross-conjugated tight-binding model systems, illustrating the various interactions. (a) Two cross-conjugated 2 site molecules. (b) Two linearly conjugated 2 site molecules. α represents the onsite energy. Arrows indicate the interactions, where β denotes the overlap integral between neighboring sites, and a and b represent the intermolecular interaction integrals. V corresponds to the coupling to the electrode, and δ is a single parameter that characterizes the through-electrode intermolecular interaction. It should be noted that δ does not correspond to a simple overlap integral. The intermolecular interactions are highlighted with red dashed arrows.

cross-conjugated (resulting in DQI) or linearly conjugated (resulting in no DQI), coupled to leads.

The choice of molecules for the model system is primarily aimed at maximizing simplicity while retaining the capability to model molecular interactions effectively. The minimal model for a cross-conjugated system, like the AQ family of molecules, is two sites where one site is connected to both electrodes and the other is connected to neither as in Figure 3a. The minimal model for a comparative linearly conjugated system is two sites where each site is connected to a single electrode, as shown in Figure 3b. To probe the effects of intermolecular interactions, we need to consider the different ways these two sites can couple to neighboring molecules. Consequently, it is essential to include two molecules in the model. In this setup, both molecules are connected to the leads. If we imagine these to be models of organic molecules, we could consider these to be ethene molecules connected directly to the leads.

Figure 3 depicts a schematic representation of the cross-conjugated system (Figure 3a) and the linear system (Figure 3b). All interactions included in the models are shown as arrows, where α is the onsite energy, β is the overlap integral and a and b are the intermolecular interaction integrals, highlighted as the red dashed arrows. In the model, each alpha corresponds to a carbon atom in the ethene molecules. Since each ethene molecule consists of two carbon atoms, there are two alphas in both cases. In the linear setup, each carbon in the ethene molecule is connected to one lead. However, in the cross-conjugated setup, only one carbon in each ethene molecule is connected to both leads

The Hamiltonians of the molecules in the two configurations are identical, and read

$$\mathbf{H} = \begin{bmatrix} \alpha & \beta & b & a \\ \beta & \alpha & a & b \\ b & a & \alpha & \beta \\ a & b & \beta & \alpha \end{bmatrix} \tag{1}$$

where α is the onsite energy, β is the overlap integral between neighboring sites, and a and b are intermolecular interaction integrals. Within a coherent tunneling formalism, the zero-bias transmission through a molecular wire at zero temperature is given as

$$T(\varepsilon) = \mathrm{Tr}\{\mathbf{\Gamma}^L \mathbf{G}(\varepsilon) \mathbf{\Gamma}^R \mathbf{G}^\dagger(\varepsilon)\} \tag{2}$$

Here, the retarded Green's function, $G(\varepsilon)$, is defined as

$$G(\varepsilon) = [\varepsilon \mathbf{I} - \mathbf{H} + \frac{i}{2}\mathbf{\Gamma}^L + \frac{i}{2}\mathbf{\Gamma}^R]^{-1} \tag{3}$$

Where ε is the energy and $\mathbf{I}$ is the unit matrix. $\mathbf{\Gamma}^L$and $\mathbf{\Gamma}^R$ describe the broadening of the molecular resonances caused by the coupling to the leads, V. Additionally, we consider the inclusion of through-electrode intermolecular interaction, represented as δ. Yaliraki and Ratner[19] have demonstrated that this interaction has an impact on the conductance when the molecules are in close proximity to each other, specifically at a distance equivalent to the unit lattice distance. The self-energies for the cross-conjugated model system (Figure 3a) read

$$\mathbf{\Gamma}^L = \mathbf{\Gamma}^R = \begin{bmatrix} V^2 & 0 & 0 & \delta \\ 0 & 0 & 0 & 0 \\ 0 & 0 & 0 & 0 \\ \delta & 0 & 0 & V^2 \end{bmatrix} \tag{4}$$

and for the linearly conjugated model system (Figure 3b),

https://doi.org/10.1021/acsnanoscienceau.4c00041
ACS Nanosci. Au 2024, 4, 426−434

$$\Gamma^L = \begin{bmatrix} V^2 & 0 & 0 & \delta \\ 0 & 0 & 0 & 0 \\ 0 & 0 & 0 & 0 \\ \delta & 0 & 0 & V^2 \end{bmatrix}, \quad \Gamma^R = \begin{bmatrix} 0 & 0 & 0 & 0 \\ 0 & V^2 & \delta & 0 \\ 0 & \delta & V^2 & 0 \\ 0 & 0 & 0 & 0 \end{bmatrix} \tag{5}$$

The total current through the system can then be calculated as

$$I = \frac{2e}{h} \int_{-\infty}^{\infty} d\varepsilon [f_L - f_R] T(\varepsilon) \tag{6}$$

where$[f_L - f_R]$ refers to the Fermi Dirac distribution for the left and right electrode and $T(\varepsilon)$ is the zero bias transmission shown in eq 2. From the total current, the zero-bias differential conductance can also be obtained by differentiation with voltage (see SI for further details).

The transmissions for the two models, considering different parameter choices, are depicted in Figure 4. To gain a deeper understanding of these results, it is necessary to examine the molecular systems in detail. The Hamiltonian has the following eigenvalues:

$$\begin{aligned} \varepsilon_1 &= \alpha + \beta - b + a, \\ \varepsilon_2 &= \alpha + \beta + b - a, \\ \varepsilon_3 &= \alpha - \beta - b - a, \\ \varepsilon_4 &= \alpha - \beta + b + a. \end{aligned} \tag{7}$$

Examining the eigenvalues provides insight into the energetic locations of the resonances in the transmission spectrum. The eigenvalues exhibit a splitting of both the occupied orbitals, ε_1 and ε_2, as well as the unoccupied orbitals, ε_3 and ε_4, when intermolecular interactions a and b are taken into account. As the values of a and b approach zero, the eigenvalues become degenerate pairs, indicating the behavior of two noninteracting molecules. This observation highlights the influence of intermolecular interactions on the electronic structure and the resonance behavior in the system.

Figure 4 presents the transmission for the linearly conjugated model systems (Figure 4a,b) and the cross-conjugated model system (Figure 4c). Both model system calculations were performed with β as −2.7 eV and α as 0 eV. The colors in the figure indicate the degree of interaction between the two molecules. The black dashed-dotted line corresponds to no interaction (a, b = 0 eV, 0 eV), representing two isolated single molecules (SM). The purple dashed line represents weak interactions (a, b = −0.1 eV, −0.05 eV), resembling two molecules with weak intermolecular interactions, while the orange solid line indicates strong interactions (a, b = −0.2 eV, −0.1 eV), resembling two molecules with strong intermolecular interactions. The purpose of illustrating weak (purple) and strong (orange) interactions is to show a sparsely packed monolayer (M) and a densely packed monolayer (DM), respectively.

The transmission through the linearly conjugated ethene system (Figure 4a,b) reveals a splitting of the molecular resonances when the coupling to the electrodes is set to a sufficiently small value, V = −0.2 eV, and δ = 0.0 eV^2 (Figure 4a). However, when the coupling is strengthened to V = −1.0 eV and δ = 0.2 eV^2, the molecular resonances become broadened, resulting in the disappearance of peak splitting (Figure 4b). Similar behavior can be observed for the resonant characteristics of the cross-conjugated ethene model system (see Figures S2 and S3). This observation aligns with the findings of Obersteiner et al.,[20] who previously reported the splitting of molecular resonances in clusters comprising only two molecules.

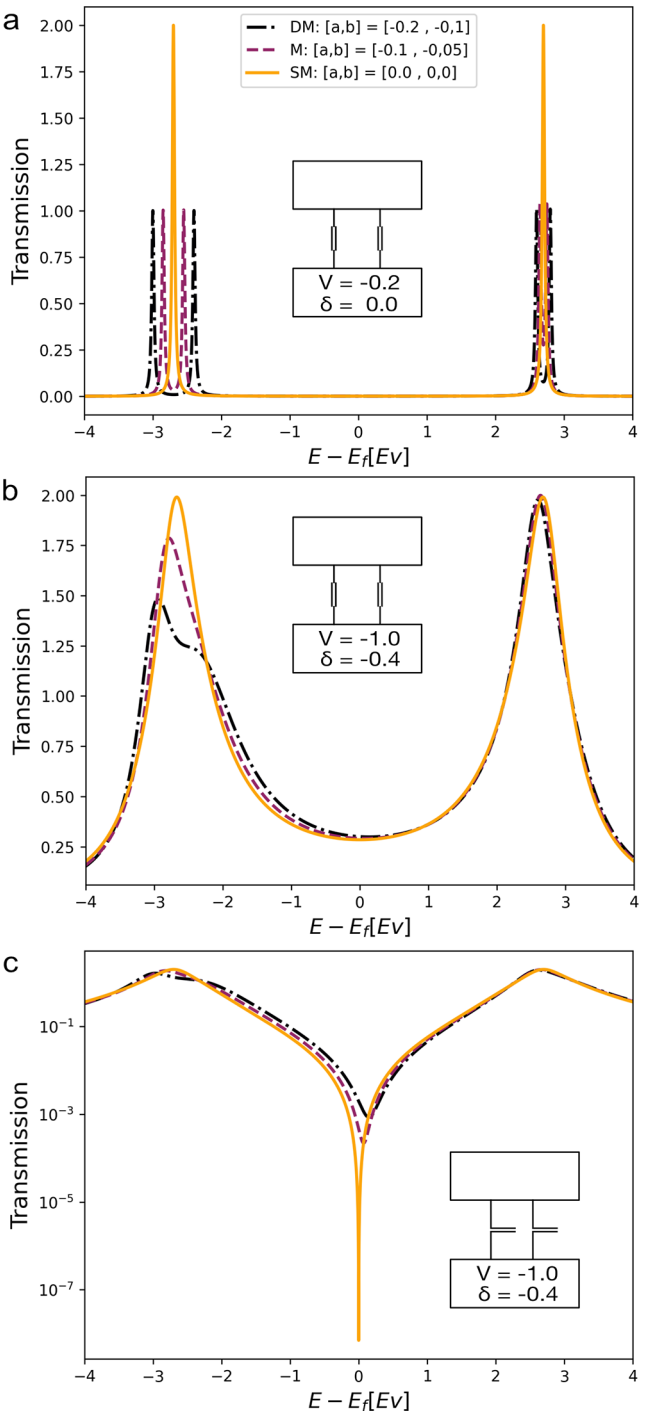

Figure 4. Energy-dependent zero-bias transmission for the linearly conjugated (a,b) and cross-conjugated (c) model systems in a strongly coupled configuration (b,c) and a weakly coupled configuration (a). The colors indicate whether the two molecules are non-interacting (black dashed−dotted line), corresponding to two isolated molecules, weakly interacting (purple dashed line), corresponding to a sparse monolayer, or strongly interacting (orange solid line) corresponding to a dense monolayer. The transmission in (c) is plotted on a logarithmic scale to highlight the effects on the antiresonance.

The linearly conjugated system cannot give us any indication of the effects of intermolecular interaction on DQI, however, in

https://doi.org/10.1021/acsnanoscienceau.4c00041
ACS Nanosci. Au 2024, 4, 426−434

Figure 4c, a noticeable dip in conductance at the Fermi energy is apparent for the cross-conjugated system.

In these model system calculations we can solve for values of energy (E) where the transmission goes to zero, and find it is purely real for noninteracting molecules in the junction. However, when we include intermolecular interactions in the Hamiltonian and self-energies, this solution becomes imaginary. Depending on the strength of the interaction, the transmission zero moves deeper into the complex plane, and consequently, the dip on the real axis becomes less pronounced (For further information, see SI). We note here that it would be interesting to have a physical interpretation for this result, but at this stage, we only have a mathematical observation.

From these calculations we conclude that both a depth reduction and shift of the antiresonance could be observed when intermolecular interactions are present. The shift in the destructive interference feature occurs due to a change in the relative positions of the HOMO and LUMO at different interaction strengths, which is a consequence of the asymmetric shift of the resonances.

Up to this point, the model has not taken into account any electrostatic interactions, and therefore, no uniform resonance shifts across the full spectrum have been observed. In actual molecular junctions, electrostatic effects arise from local dipoles associated with the linker groups, leading to changes in the local electrostatic environment.[21] To incorporate this effect into the model, the on-site energies, denoted as α, can be shifted. This shift in α results in a corresponding shift in the transmission spectrum, as depicted in Figure 5a. Here, the transmission of the dense monolayer is plotted for different α values: 0.0, 0.5, and 1.0. It is worth noting that the shift in transmission and the position of the antiresonance significantly influence the line shape of the conductance, as demonstrated in Figure 5b. When an antiresonance in the transmission approaches the Fermi level, a sharp dip in the conductance occurs. The magnitude of this conductance dip depends on the depth and location of the antiresonance in the transmission, given that the conductance is calculated based on the transmission at the Fermi energy.

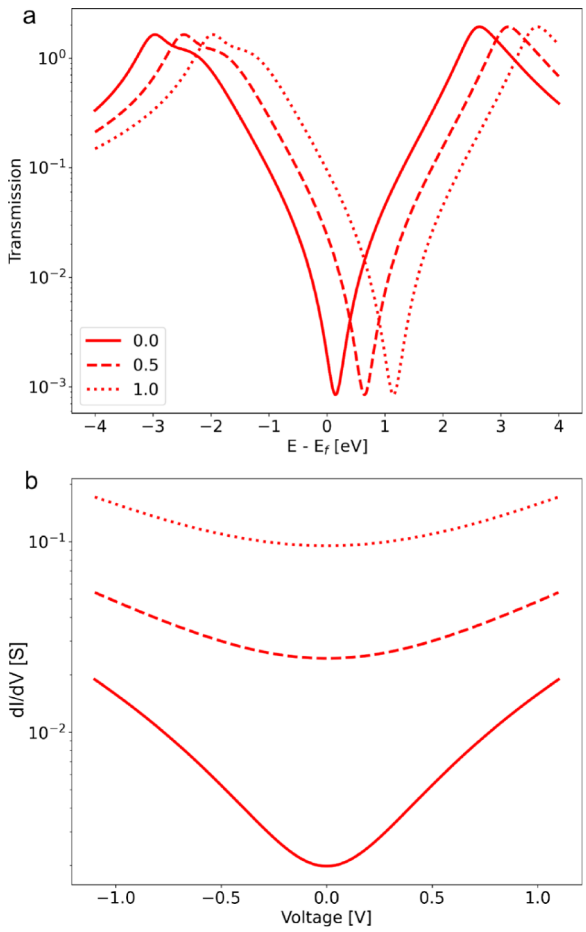

Figure 5. Energy-dependent zero-bias transmission (a) and corresponding dI/dV curves (b) for the cross-conjugated model system. The calculations are performed at different onsite energies: 0.0, 0.5, and 1.0. The figure emphasizes the sensitivity of dI/dV to the position and depth of the antiresonance in the transmission. The $I-V$ traces are calculated from the energy-dependent zero-bias transmission function according to eq 6, and the dI/dV traces are obtained from differentiation of the $I-V$ curves.

ATOMISTIC CALCULATIONS

Following the model system, we extended our investigation to include three conjugated molecules, namely, AQ-MT, AQ-DT, and AC-DT, which were incorporated into an Au−molecule−Au junction (Figures S4 and S5). Our interest was focused on understanding how the interactions between these molecules would impact the electronic transmission. To guide our study, we drew inspiration from the work conducted by Obersteiner et al.[20] They investigated charge transport through molecular clusters that do not exhibit interference and observed a highly nonlinear current behavior as the clusters increased in size. They attributed this behavior to the collective electrostatic effects originating from the dipoles associated with the binding groups. Their work emphasized the significant influence of the transition from a single molecule to a cluster on the overall current. Motivated by their findings, we probe the impact of intermolecular interactions on the transition from single molecules to monolayers in systems with DQI.

We calculate the transmission for various junction configurations, ranging from a single molecule (SM) to clusters consisting of 4 (C4), 6 (C6), and 9 (C9) molecules as well as dense monolayer (DM) and sparse monolayer (M) configurations. For the monolayer calculations, we treated the system as one molecule within a small unit cell and applied periodic boundary conditions. Additionally, we conducted calculations for a sparse monolayer junction with 4 molecules included explicitly in the unit cell, representing the same density as the one-molecule sparse monolayer configuration.

Figure 6 provides an illustration of the different junction configurations with the top electrode removed for clarity. The dots in the figure indicate the positions of the binding group, while the lines represent the size of the unit cell for each junction configuration. In Figure 6a, the solid red line represents a densely packed monolayer consisting of a single molecule on a 2 × 2 Au FCC(111) electrode. In addition, the dotted red line represents a sparse monolayer, consisting of one molecule on a (3 × 3) Au FCC(111) electrode. For the single molecule and cluster configurations, we modeled the systems with 1 (4, 6, or 9) molecule(s) on a (9 × 9) Au FCC(111) electrode.

The molecules in the junctions are positioned at every second FCC hollow sites, resulting in a distance of 5.77 Å between the sulfur atoms of neighboring molecules. This arrangement leads to different molecular coverages for each configuration: SM (single molecule) has a coverage of $\frac{1}{16}$, C4

https://doi.org/10.1021/acsnanoscienceau.4c00041
ACS Nanosci. Au 2024, 4, 426−434

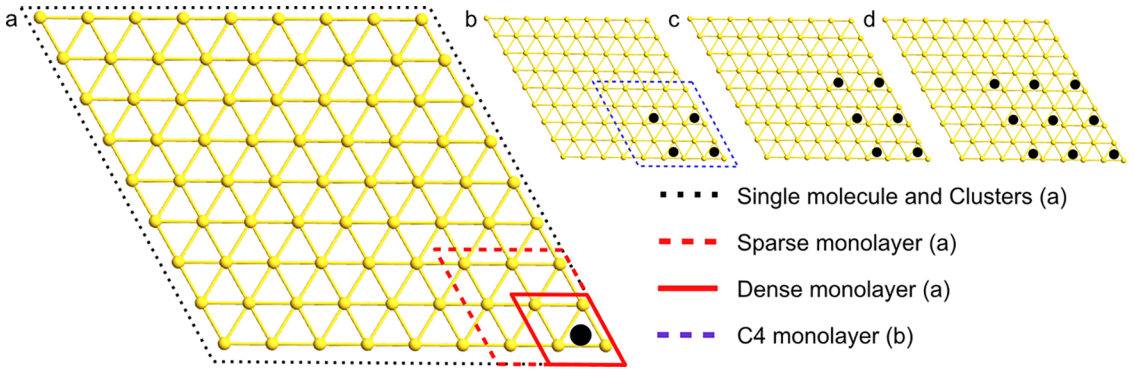

Figure 6. Illustration of the different junction configurations. The top gold electrode is removed for clarity. The black dots represent a molecule location, while the dotted/solid lines represent the different electrode size. If no line is present, the electrode is the size of the entire Au surface. The single molecules and clusters are all added to a 9 × 9 Au electrode. The following configurations are depicted: (a) Single molecule (SM) and dense (DM)/sparse (M) monolayer. The single molecule electrode is shown as a dotted black line. The dense and sparse monolayer electrodes are the solid and dotted red line, respectively. The single molecule is on a 9 × 9 Au electrode, whereas the sparse and dense monolayer consists of a single molecule on a 2 × 2 and 3 × 3 Au electrode, respectively. (b) Four-molecule cluster (C4) and four-molecule monolayer (C4M): The electrode of the C4 monolayer is indicated by a dotted line (5 × 5 Au electrode). (c) 6 molecule cluster (C6). (d) 9 molecule cluster (C9).

(cluster of 4 molecules) has a coverage of $\frac{4}{16}$, C6 (cluster of 6 molecules) has a coverage of $\frac{6}{16}$, and C9 (cluster of 9 molecules) has a coverage of $\frac{9}{16}$. It is worth noting that our chosen molecular coverage differs from that used by Obersteiner et al., as they employed a smaller electrode, which resulted in closer proximity of the molecules in their junctions. Illustrations of the molecular density for SM, C4, C6, and C9 can be found in Figure 6a–d, respectively.

To simulate a sparse monolayer junction with 4 molecules (C4M), we selected a (5 × 5) Au FCC(111) electrode with 4 molecules in the junction. This choice was made to mimic the density of the single-molecule sparse monolayer. From this point onward, we will refer to this configuration as the C4 monolayer (C4M). Further details regarding the calculation setup can be found in Section S2).

To investigate how the molecular environment affects the transmission, we calculated the transmission per molecule for each junction configuration, ranging from a single molecule to a dense monolayer. We were particularly interested in examining the impact of the electrostatic interactions, which we knew from the model system would result in a resonance shift. The results of these calculations are presented in Figure 7. In each plot, the triangular marks show the lowest transmission value for each system, and a vertical line is included to highlight their position on the energy axis. The corresponding transmission spectra for each junction setup are shown in the same colors but faded in the background. For the linear-conjugated molecule AC-DT (Figure 7a), no DQI features are observed in the transmission. This aligns with our expectations based on the model system. In contrast, when examining the cross-conjugated molecules AQ-DT and AQ-MT (Figure 7b,c, respectively), DQI features are observed in the transmission spectra, and they are shifted toward higher energy with intermolecular interactions. These observations are consistent with our model system predictions. We cannot definitively determine why the energy of the single molecule junctions exhibits an antiresonance at a specific position. However, we can assert that the energy of the system is influenced by intermolecular interactions, which become apparent when more molecules are added to the junction.

The transmission decreases going from AC-DT to AQ-DT and further to AQ-MT. This reduction in transmission is first due the absence/presence of DQI but can be partially attributed to the variations in the binding groups utilized. AC-DT and AQ-DT both feature sulfur (S) as the binding group on both sides of the molecule, and it is widely acknowledged in the literature that sulfur and gold exhibit a strong interaction.[22] On the other hand, AQ-MT incorporates a sulfur binding group on one side and a hydrogen atom on the other side, resulting in weaker coupling between one side of the molecule and the electrode.

While the difference in binding group contributes slightly to the change in transmission, the primary factor contributing to the overall decrease in transmission is the presence of DQI. In addition to the evident dip in the transmission spectrum, DQI further diminishes the transmission compared with that of the linearly conjugated molecule.

First, examining the magnitude of the transmission per molecule for the cross-conjugated molecules AQ-DT and AQ-MT, we see that both the single molecule (SM) and the sparse monolayer (M) exhibit similar low levels of transmission at their minima (triangles). Given this similarity in minimum transmission levels and the absence of intermolecular interactions in a single molecule, it suggests that the primary factor responsible for the dip shift lies within the molecular environment.

Since we cannot entirely dismiss the possibility of electrode effects, we calculated the electrostatic difference potential (EDP) (see Supporting Information). This calculation allows us to examine how the charge rearrangement in the junction changes the potential. We do observe a charge rearrangement at the electrode–molecule interface, with the molecule becoming increasingly negatively charged as the number of molecules in a cluster or the density of the monolayer increases. These types of charge rearrangements will certainly result in orbital energy shifts, although we cannot quantify to what extent this affects the shift of the interference feature. We emphasize that the electrodes are periodic for all systems, with additional gold atoms added for the cluster calculations to minimize cluster–cluster interactions. Essentially, the cluster calculations represent dilute monolayers of clusters.

https://doi.org/10.1021/acsnanoscienceau.4c00041
ACS Nanosci. Au 2024, 4, 426–434

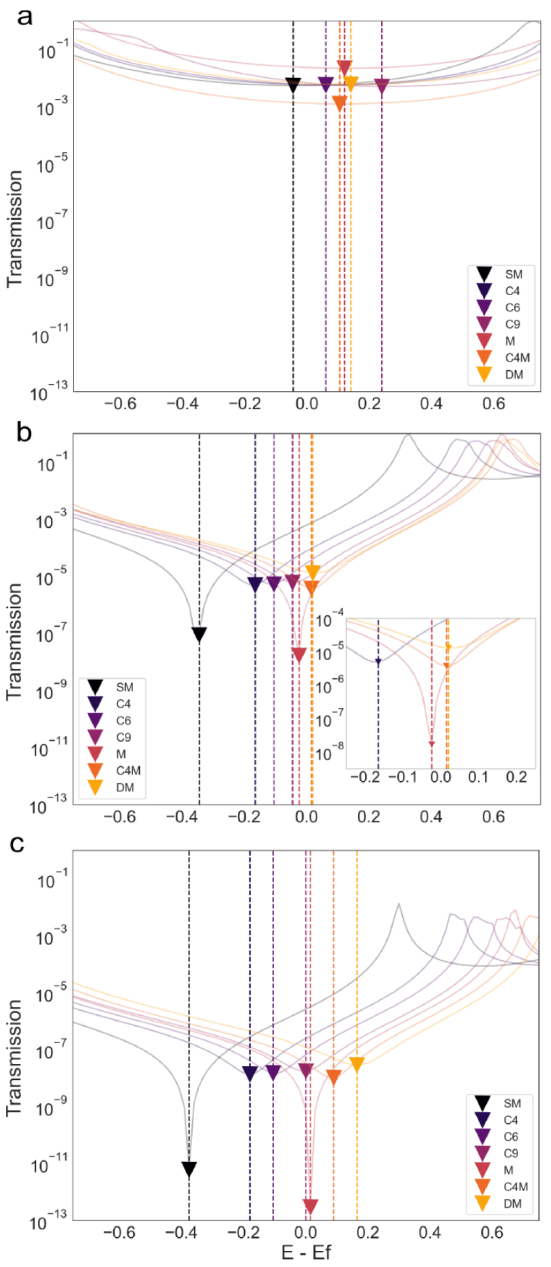

Figure 7. Energy-dependent zero-bias transmission spectra for each molecule: AC-DT (a), AQ-DT (b), and AQ-MT (c), calculated with DFT. In each spectrum, the marks highlight the lowest point of transmission. Additionally, the shifts in the transmission features are emphasized by vertical dashed lines, providing visual cues for the changes in the transmission characteristics.

To further investigate the effect of the molecular environment, we can examine the calculations for the C4 monolayer (C4M), which represents a molecular density equivalent to that of a sparse monolayer (one molecule on a 3 × 3 Au electrode). If the complete influence of the molecular environment is accounted for in the sparse monolayer (M), the transmission spectra of the sparse monolayer (M) and the C4 monolayer (C4M) should be identical. Conversely, if the two curves diverge, it would indicate a deviation due to the molecular environment.

In Figure 7b (AQ-DT), the inset provides a magnified view of the transmission spectra for the four-cluster (C4), C4 monolayer (C4M), sparse monolayer (M), and dense monolayer (DM) configurations. This illustration serves to highlight that the C4 monolayer (C4M) and sparse monolayer (M) are not identical. This disparity indicates that when modeling a monolayer with a single molecule and periodic boundary conditions (M), some information regarding molecular interactions is lost. Furthermore, the 4 cluster (C4) and C4 monolayer (C4M) possess the same features. The resonance is merely shifted as a result of the change in the molecular environment when we shift from a small cluster of molecules to a monolayer junction.

The dense monolayer (DM) exhibits a transmission curve that resembles the clusters but with a higher overall transmission. In the case of AQ-MT (Figure 7c), the dense monolayer (DM) also undergoes a further energy shift upward. This suggests that unsurprisingly, the dense monolayer (DM) experiences stronger interactions with the surrounding molecules compared to the sparse monolayer (M). However, whether the molecules would pack together so densely in an experimental scenario remains to be determined. These findings emphasize the critical importance of simulating junctions as accurately as possible when considering intermolecular interactions. By capturing the realistic molecular environment, we can obtain a more comprehensive understanding of the transmission behavior and its dependence on molecular packing.

It is important to note that the atomistic calculations do not allow us to distinguish between electrostatic effects and screening effects from neighboring molecules. Therefore, it is challenging to definitively conclude whether screening plays a role in the observed DQI without further investigation or experimental validation. However, it is worth noting that even if screening does influence DQI, its impact ultimately stems from the molecular environment.

To establish a comparison with experimental measurements, we focused on calculating the differential conductance based on the transmission at the Fermi energy for both the single-molecule (SM) and the C4 monolayer (C4M) of AQ-DT and AQ-MT. Figure 8 illustrates the transmission (Figure 8a) and the corresponding differential conductance (Figure 8b) for AQ-DT and AQ-MT. As observed, similar to the model system, the C4 monolayer (C4M) exhibits a dip in both the transmission near the Fermi energy and the differential conductance. Conversely, the single molecule (SM), which displays a sharp dip at lower energies in the transmission, does not show a corresponding dip in the differential conductance. These results highlight the significance of the DQI position within the transmission spectrum in determining whether a clear direct signature of DQI is experimentally observed in the differential conductance.

It is crucial to acknowledge the caveats regarding the molecular environment. This could arise from using a single molecule calculation to interpret a monolayer experiment, uncertainties in monolayer density or packing, or the potential influence of additional molecules on what would be considered a single molecule. In all cases, the exact energetic position of the antiresonance dips cannot be known precisely, and the correspondence between theory and experiments must be interpreted accordingly. However, by analyzing trends present in the calculations, we can gain valuable insights into the behavior of different molecules.

https://doi.org/10.1021/acsnanoscienceau.4c00041
ACS Nanosci. Au 2024, 4, 426−434

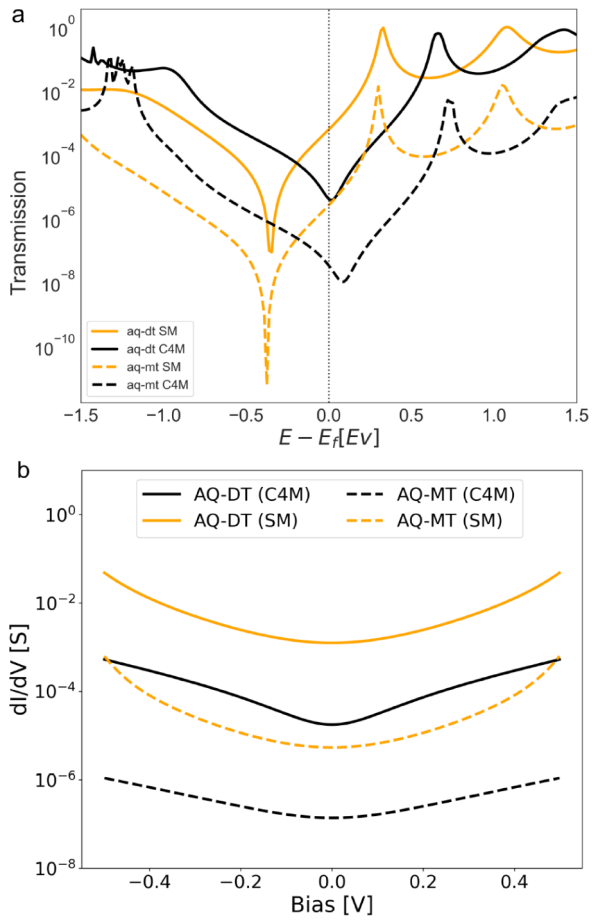

Figure 8. Zero-bias transmission spectra of AQ-DT (solid line) and AQ-MT (dashed line) in both single molecule and C4 monolayer junction configurations (a). The color scheme distinguishes between the calculation performed on a single molecule (SM, indicated by orange) and a C4 monolayer (C4M, indicated by black). Simulated dI/dV traces (b) were calculated from the zero-bias transmission function. These dI/dV traces are obtained through differentiation of the integrated transmission function, as specified by eq 6.

CONCLUSION

This work presents a comprehensive investigation of a group of molecules with and without DQI and the role of intermolecular interactions in controlling the observed transport properties. The key findings emphasize the influence of the molecular environment on the presence and manifestation of DQI. Shifting from single molecules to monolayers, which alters the molecular interactions within the junction, can lead to a shift of an antiresonance toward higher energy. This explains why single molecules may not exhibit a direct signature of DQI in experimental measurements even if this is observed in monolayers measurements. Additionally, the study highlights the significance of considering intermolecular interactions in simulating junctions. The results demonstrate that the transmission can be significantly impacted when transitioning from a one-molecule junction to a junction with four molecules while maintaining the same molecular density and applying periodic boundary conditions. By advancing our understanding of how intermolecular interactions affect properties, such as DQI, this work provides guidelines for best practice for calculations of monolayer experiments and the interpretation of agreement, or lack thereof, between calculations, single-molecule experiments, and monolayer experiments on the same molecule.

METHOD

The calculations were conducted by using density functional theory (DFT) combined with the Greens function approach and the Landauer formula to determine the transmission and conductance. QuantumATK (version S-2021.06-SP1)[23−25] was employed for these calculations, utilizing the GGA PBE functional.[26,27] A double-ζ basis set (with a single-ζ on Au) and polarization functions on all molecular atoms were used along with periodic boundary conditions. Additionally, noncovalent interactions were accounted for by incorporating the Grimme DFT D3 dispersion correction.[28] Further details regarding the calculations can be found in the Supporting Information.

ASSOCIATED CONTENT

Supporting Information

The Supporting Information is available free of charge at https://pubs.acs.org/doi/10.1021/acsnanoscienceau.4c00041.

Atomistic calculations details. Additional model system calculations, including figures of the cross conjugated system strongly coupled, the cross conjugated system weakly coupled, and the linear conjugated system strongly coupled (on a logarithmic scale). Explanation of the differentiation of the total current. Calculated energy at the transmission minimas of the model system. Electrostatic difference potential (EDP) (PDF)

AUTHOR INFORMATION

Corresponding Author

Gemma C. Solomon − *Department of Chemistry and Nano-Science Center, University of Copenhagen, Copenhagen 2100, Denmark; NNF Quantum Computing Programme, Niels Bohr Institute, University of Copenhagen, Copenhagen 2100, Denmark;* orcid.org/0000-0002-2018-1529; Email: gsolomon@chem.ku.dk

Authors

Louise O. H. Hyllested − *Department of Chemistry and Nano-Science Center, University of Copenhagen, Copenhagen 2100, Denmark;* orcid.org/0000-0002-1701-0438

Idunn Prestholm − *Department of Chemistry and Nano-Science Center, University of Copenhagen, Copenhagen 2100, Denmark*

Complete contact information is available at: https://pubs.acs.org/10.1021/acsnanoscienceau.4c00041

Author Contributions

CRediT: **Louise Oxen Høgh Hyllested** conceptualization, data curation, formal analysis, methodology, project administration, visualization, writing - original draft, writing - review & editing; **Idunn Prestholm** conceptualization, data curation, formal analysis, methodology, visualization, writing - original draft, writing - review & editing; **Gemma C. Solomon** conceptualization, funding acquisition, methodology, supervision, writing - review & editing.

Notes

The authors declare no competing financial interest.

https://doi.org/10.1021/acsnanoscienceau.4c00041
ACS Nanosci. Au 2024, 4, 426−434

■ ACKNOWLEDGMENTS

We would like to acknowledge the European Research Council (ERC) for their generous funding of this project under the European Union's Horizon 2020 research and innovation programme (grant agreement No. 865870). Additionally, we would like to acknowledge the use of ChatGPT for its assistance in making grammatical corrections throughout the writing process.

■ REFERENCES

(1) Arroyo, C. R.; Tarkuc, S.; Frisenda, R.; Seldenthuis, J. S.; Woerde, C. H. M.; Eelkema, R.; Grozema, F. C.; Van Der Zant, H. S. Signatures of quantum interference effects on charge transport through a single benzene ring. *Angew. Chem., Int. Ed.* **2013**, *52*, 3152−3155.

(2) Liu, Y.; Ornago, L.; Carlotti, M.; Ai, Y.; El Abbassi, M.; Soni, S.; Asyuda, A.; Zharnikov, M.; van der Zant, H. S. J.; Chiechi, R. C. Intermolecular Effects on Tunneling through Acenes in Large-Area and Single-Molecule Junctions. *J. Phys. Chem. C* **2020**, *124*, 22776−22783.

(3) Zotti, L. A.; Leary, E. Taming quantum interference in single molecule junctions: Induction and resonance are key. *Phys. Chem. Chem. Phys.* **2020**, *22*, 5638−5646.

(4) Guédon, C. M.; Valkenier, H.; Markussen, T.; Thygesen, K. S.; Hummelen, J. C.; Van Der Molen, S. J. Observation of quantum interference in molecular charge transport. *Nat. Nanotechnol.* **2012**, *7*, 305.

(5) Aradhya, S. V.; Meisner, J. S.; Krikorian, M.; Ahn, S.; Parameswaran, R.; Steigerwald, M. L.; Nuckolls, C.; Venkataraman, L. Dissecting contact mechanics from quantum interference in single-molecule junctions of stilbene derivatives. *Nano Lett.* **2012**, *12*, 1643−1647.

(6) Arroyo, C. R.; Tarkuc, S.; Frisenda, R.; Seldenthuis, J. S.; Woerde, C. H.; Eelkema, R.; Grozema, F. C.; van der Zant, H. S. Signatures of quantum interference effects on charge transport through a single benzene ring. *Angew. Chem.* **2013**, *125*, 3234−3237.

(7) Liu, X.; Sangtarash, S.; Reber, D.; Zhang, D.; Sadeghi, H.; Shi, J.; Xiao, Z.-Y.; Hong, W.; Lambert, C. J.; Liu, S.-X. Gating of quantum interference in molecular junctions by heteroatom substitution. *Angew. Chem., Int. Ed.* **2017**, *56*, 173−176.

(8) Ballmann, S.; Härtle, R.; Coto, P. B.; Elbing, M.; Mayor, M.; Bryce, M. R.; Thoss, M.; Weber, H. B. Experimental evidence for quantum interference and vibrationally induced decoherence in single-molecule junctions. *Phys. Rev. Lett.* **2012**, *109*, 056801.

(9) Garner, M. H.; Li, H.; Chen, Y.; Su, T. A.; Shangguan, Z.; Paley, D. W.; Liu, T.; Ng, F.; Li, H.; Xiao, S.; et al. Comprehensive suppression of single-molecule conductance using destructive σ-interference. *Nature* **2018**, *558*, 415−419.

(10) Huang, B.; Liu, X.; Yuan, Y.; Hong, Z. W.; Zheng, J. F.; Pei, L. Q.; Shao, Y.; Li, J. F.; Zhou, X. S.; Chen, J. Z.; Jin, S.; Mao, B. W. Controlling and Observing Sharp-Valleyed Quantum Interference Effect in Single Molecular Junctions. *J. Am. Chem. Soc.* **2018**, *140*, 17685−17690.

(11) Bai, J.; et al. Anti-resonance features of destructive quantum interference in single-molecule thiophene junctions achieved by electrochemical gating. *Nat. Mater.* **2019**, *18*, 364−369.

(12) Zhang, Y.; Ye, G.; Soni, S.; Qiu, X.; Krijger, T. L.; Jonkman, H. T.; Carlotti, M.; Sauter, E.; Zharnikov, M.; Chiechi, R. C. Controlling destructive quantum interference in tunneling junctions comprising self-assembled monolayers via bond topology and functional groups. *Chem. Sci.* **2018**, *9*, 4414−4423.

(13) Fracasso, D.; Valkenier, H.; Hummelen, J. C.; Solomon, G. C.; Chiechi, R. C. Evidence for quantum interference in SAMs of arylethynylene thiolates in tunneling junctions with eutectic Ga−In (EGaIn) top-contacts. *J. Am. Chem. Soc.* **2011**, *133*, 9556−9563.

(14) Rabache, V.; Chaste, J.; Petit, P.; Della Rocca, M. L.; Martin, P.; Lacroix, J.-C.; McCreery, R. L.; Lafarge, P. Direct observation of large quantum interference effect in anthraquinone solid-state junctions. *J. Am. Chem. Soc.* **2013**, *135*, 10218−10221.

(15) Carlotti, M.; Kovalchuk, A.; Wächter, T.; Qiu, X.; Zharnikov, M.; Chiechi, R. C. Conformation-driven quantum interference effects mediated by through-space conjugation in self-assembled monolayers. *Nat. Commun.* **2016**, *7*, 13904.

(16) Chen, X.; Kretz, B.; Adoah, F.; Nickle, C.; Chi, X.; Yu, X.; Del Barco, E.; Thompson, D.; Egger, D. A.; Nijhuis, C. A. A single atom change turns insulating saturated wires into molecular conductors. *Nat. Commun.* **2021**, *12*, 3432.

(17) Lykkebo, J.; Gagliardi, A.; Pecchia, A.; Solomon, G. C. IETS and quantum interference: Propensity rules in the presence of an interference feature. *J. Chem. Phys.* **2014**, *141*, 124119.

(18) Solomon, G. C.; Herrmann, C.; Hansen, T.; Mujica, V.; Ratner, M. A. Exploring local currents in molecular junctions. *Nat. Chem.* **2010**, *2*, 223−228.

(19) Yaliraki, S. N.; Ratner, M. A. Molecule-interface coupling effects on electronic transport in molecular wires. *J. Chem. Phys.* **1998**, *109*, 5036−5043.

(20) Obersteiner, V.; Huhs, G.; Papior, N.; Zojer, E. Unconventional Current Scaling and Edge Effects for Charge Transport through Molecular Clusters. *Nano Lett.* **2017**, *17*, 7350−7357.

(21) Obersteiner, V.; Egger, D. A.; Heimel, G.; Zojer, E. Impact of collective electrostatic effects on charge transport through molecular monolayers. *J. Phys. Chem. C* **2014**, *118*, 22395−22401.

(22) Bain, C. D.; Troughton, E. B.; Tao, Y. T.; Evall, J.; Whitesides, G. M.; Nuzzo, R. G. Formation of monolayer films by the spontaneous assembly of organic thiols from solution onto gold. *J. Am. Chem. Soc.* **1989**, *111*, 321−335.

(23) Synopsis *QuantumATK version S-2021.06-SP1*. www.synopsys.com/silicon/quantumatk.html, Accessed 2023 February 6.

(24) Soler, J. M.; Artacho, E.; Gale, J. D.; García, A.; Junquera, J.; Ordejón, P.; Sánchez-Portal, D. The SIESTA method for ab initio order-N materials simulation. *J. Phys.: Condens. Matter* **2002**, *14*, 2745.

(25) Brandbyge, M.; Mozos, J.-L.; Ordejón, P.; Taylor, J.; Stokbro, K. Density-functional method for nonequilibrium electron transport. *Phys. Rev. B* **2002**, *65*, 165401.

(26) Burke, K.; Perdew, J.; Ernzerhof, M. Generalized Gradient Approximation Made Simple. *Phys. Rev. Lett.* **1997**, *78*, 1396.

(27) Perdew, J. P.; Burke, K.; Ernzerhof, M. Generalized Gradient Approximation Made Simple. *Phys. Rev. Lett.* **1996**, *77*, 3865.

(28) Grimme, S.; Antony, J.; Ehrlich, S.; Krieg, H. A consistent and accurate ab initio parametrization of density functional dispersion correction (DFT-D) for the 94 elements H-Pu. *J. Chem. Phys.* **2010**, *132*, 154104.

https://doi.org/10.1021/acsnanoscienceau.4c00041
ACS Nanosci. Au 2024, 4, 426−434